JOURNAL OF SOLID STATE CHEMISTRY **130,** 199–212 (1997)
ARTICLE NO. SC967141

Defect Energetics and Nonstoichiometry in Lanthanum Magnesium Hexaaluminate

Jae-Gwan Park[1] and A. N. Cormack

New York State College of Ceramics at Alfred University, Alfred, New York 14802

Received September 5, 1995; in revised form September 9, 1996; accepted September 10, 1996

Computer-based atomistic simulation methods are applied to address quantitatively the defect energetics and crystal chemistry of lanthanum magnesium hexaaluminate (LMA). The tetrahedral site preference of Mg in the magnetoplumbite structure is determined by calculating lattice energies for different Mg ion distributions. It is revealed that the intrinsic and extrinsic disorders are much influenced by the distribution of Mg in the structure. Our calculations show that oxygen Frenkel disorder is the dominant defect mode to be expected, even though Schottky disorder may also exist. Several feasible defect processes in nonstoichiometric LMA are determined from the enthalpies of the quasi-chemical reactions for the processes with simple point defect energies. We have also modeled some defect complexes in the mirror plane regions. It is found that the Mg ions positioned in the tetrahedral sites suppress the formation of cation vacancies in the mirror plane, through hindering the relaxation of the 12*k* Al ions by which the vacancies are stabilized. In Mg-deficient nonstoichiometric LMA, however, it is expected that the defect complex $[V_{La}+V_{Al}+2(V_{Al}+Al_i)]$ will be formed in the interspinel layer. Our calculations also indicate that the O_{La} defect is improbable in LMA not only as a simple point defect but also as a member of a defect complex. © 1997 Academic Press

1. INTRODUCTION

Lanthanum magnesium hexaaluminate (LMA, ideal composition $LaMgAl_{11}O_{19}$) is currently of interest as a high-efficiency host material for the active elements of solid-state lasers (1–5). The first structural analysis on LMA undertaken by Kahn *et al.* (6) confirmed that the structure was close to that of magnetoplumbite (MP, $PbFe_{12}O_{19}$) (space group $P6_3/mmc$) (7), as previously assumed from powder diffraction studies (8). The unit cell structure of strontium aluminate magnetoplumbite, $SrAl_{12}O_{19}$, is shown in Fig. 1. In their structural refinement, it was reported that the material could be slightly substoichiometric in La ion or a small amount of La ion could be localized elsewhere in the structure (the La site was only about 96% occupied). Abrahams *et al.* (9) claimed that LMA is nonstoichiometric with the formula $La_{1-x}MgAl_{11+x}O_{19}$ ($x = 0.0502$); the La deficiency is exactly compensated by excess Al. Mainly based on luminescence data, Stevels (10) proposed a nonstoichiometry $La_{1-x}MgAl_{11+5x/3}O_{19+x}$ where some oxygens are in "vacant" La sites.

There have also been several experimental reports on nonstoichiometries in systems closely related to LMA. Gasperin *et al.* (11) reported that a whole series of single crystals with $LaMn_xAl_{11}O_{18+x}$ ($0 < x < 1$) as a starting composition is obtained, and for $x \sim 1$, the crystal growth becomes much easier and resulting crystals have a good crystallinity. For lanthanum hexaaluminate (LHA, ideal composition $LaAl_{11}O_{18}$) which does not contain divalent cations, a number of stoichiometries have been reported, typically, $LaAl_{11}O_{18}$ (12), $La_{0.827}Al_{11.9}O_{19.09}$ (13), $La_{0.85}Al_{11.55}O_{18.60}$ (11), $La_{1-x}Al_{11+2/3+x-y}O_{19-3y/2}$ (14), $La_{1-x}Al_{11+2/3+x}O_{19}$ (15), and $La_{1-x}Al_{11+2/3+5x/3}O_{19+x}$ (10, 16). Iyi *et al.* proposed an MP-type structural model, the "vacancy model," having a stoichiometry of $La_{0.83}Al_{11.83}O_{19}$, based on the results of structural refinement and chemical analysis. Our recent simulation study (17) revealed that this MP-structured phase is energetically most favored, even though some other phases may exist as metastable phases.

It is obvious that, due to the complexity of the basic crystal structure of MP-type compounds, the knowledge of the nonstoichiometries and defect energetics available from experiment is quite limited. In one of our earlier simulation studies (18), several feasible defect reactions to explain its nonstoichiometry were proposed and some defect complexes which may exist in LMA were modeled. However, we have concluded that the potential model used in the earlier study was not sufficiently optimized, as discussed recently (19). In addition, it is realized that the intrinsic and extrinsic disorders in LMA are much influenced by the distribution of Mg in the structure. This effect was not considered in the

[1] To whom correspondence should be addressed. Present address: Division of Ceramics, Korea Institute of Science and Technology, P.O. Box 131, Cheongryang, Seoul 130-650, Korea.

0022-4596/97 $25.00

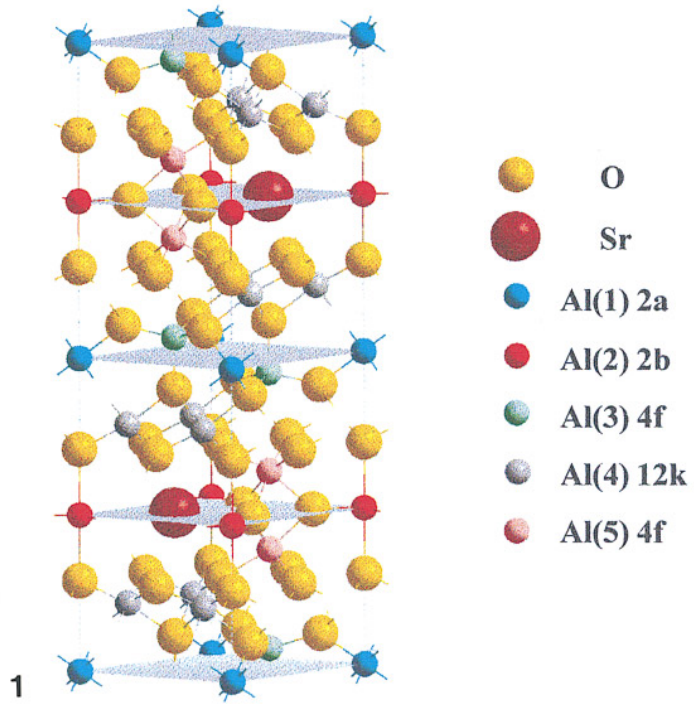

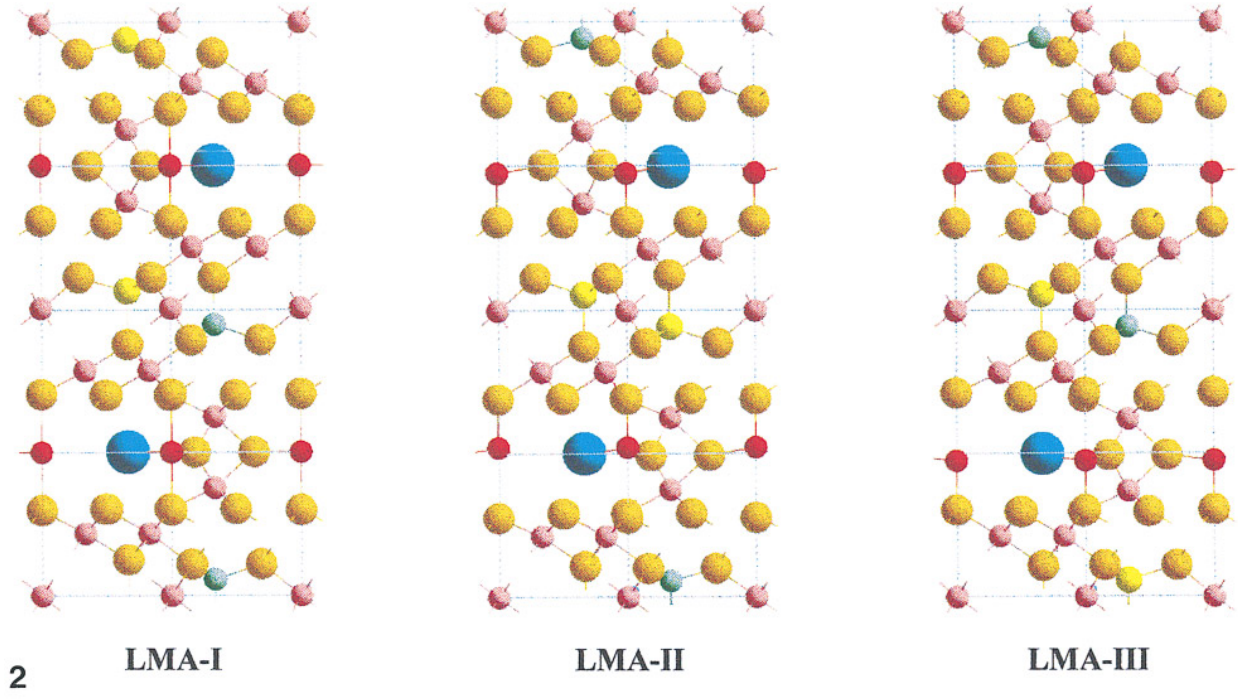

FIG. 1. Unit cell structure of Sr aluminate magnetoplumbite, $SrAl_{12}O_{19}$.

FIG. 2. [110] directional views of the equilibrated unit cell structures of LMA having distinct Mg distributions among the tetrahedral sites, showing the diverse positional behavior of Al(2) cations. (Blue = La; Orange = O; Yellow = Mg; Green = Al(3); Pink = Al in octahedral sites; Red = Al(2)).

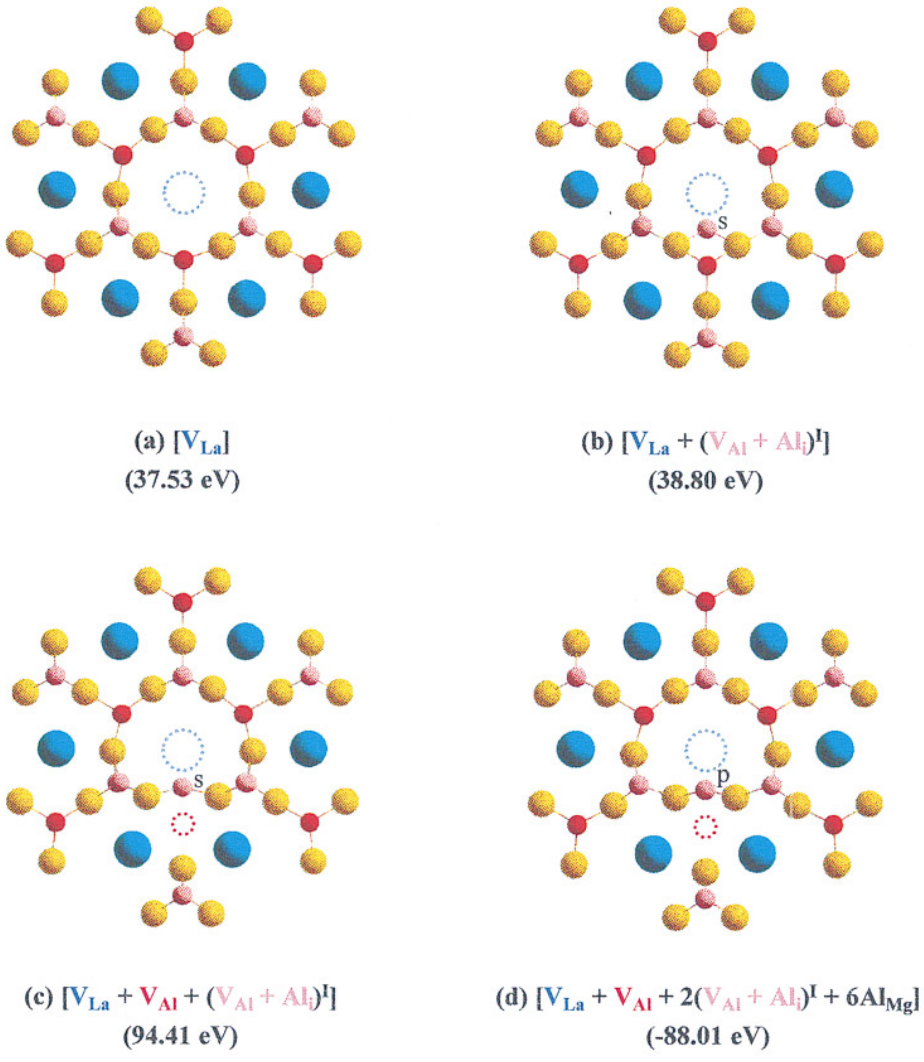

FIG. 3. [001] directional views of the equilibrated mirror plane region structures around defect(s) involving V_{La}. The energies in parentheses are the formation energies of the defect(s) expressed in brackets. (V_{Al} + Al_i)^I denotes the Frenkel-like defect relaxing from spinel block 12*k* site to mirror plane region. In (d) the six Al_{Mg}'s are positioning in neighboring spinel blocks. (Blue = La; Orange = O; Pink = Al(5) (above and below the mirror plane; overlapping); Pink with *s* = the single Al_i of the Frenkel defect; Pink with *p* = the overlapping Al_i pair of the Frenkel defects; Red = Al(2); and the dotted circles = vacancies in the mirror plane).

earlier study. Therefore, in this paper, as an extension of the earlier work and as part of our systematic study on the structure, stoichiometry, and stability in hexaaluminates, we investigate extensively the defect energetics and nonstoichiometry in LMA (focusing on the effect of the Mg distribution), using theoretical, computer-based atomistic simulation techniques with potential models more optimized than the earlier ones. Some of the topics on LMA, such as the site preference of Mg and the effect of Mg distribution on the MP structure, studied in our earlier simulation works (20, 21), are also revisited in this paper.

2. SIMULATION TECHNIQUES

2.1. Potential Models

The simulations in this study are based on the Born model description of solid, which treats the solid as a collection of point ions with short range forces acting between them. The approach has enjoyed a wide range of success, but it has been found that the reliability of the simulations depends on the validity of the potential model used in the calculations.

The short range potentials are usually described by a simple analytical Buckingham function,

$$V_{ij}(r_{ij}) = A_{ij}\exp(-r_{ij}/\rho_{ij}) - C_{ij}r_{ij}^{-6}, \quad [1]$$

where r_{ij} is the distance between the ions i and j.

The polarizability of individual ions is included through the shell model originally developed by Dick and Overhauser (22), in which the outer valence electron cloud of the ion is simulated by a massless shell of charge Y and the nucleus and inner electrons by a core of charge X. The total charge of the ion is, thus, $X + Y$ which equals the oxidation state of the ion. The interaction between core and shell of any ion is harmonic with a spring constant k, and is given by

$$V_i(r_i) = 1/2k_i d_i^2, \quad [2]$$

where d_i is the relative displacement of core and shell of ion i.

For the shell model, the value of the free-ion electronic polarizability is given by

$$\alpha_i = Y_i^2/k_i. \quad [3]$$

The potential parameters A, ρ, and C in Eq. [1], the shell charges Y, and spring constant k, associated with the shell-model description of polarizability, need to be determined for each interaction and ion type in the crystal. In the present study, they were taken from the compilation of Lewis and Catlow (23) and are listed in Table 1. The La–O and O–O parameters were taken from the works of Butler *et al.* (24) and Catlow (25), respectively. The viability of these potential models for hexaaluminates was fully discussed recently (19). It was shown that the potential models, with a consideration of the effect of coordination number of the short range potential only within the spinel blocks, yielded reasonable simulation results for the thermodynamic stabilities of alkaline earth hexaaluminates, as well as for reproducing the complex crystal structure of strontium magnetoplumbite.

TABLE 1
Interatomic Potential Parameters Used in This Study

(a) Short-range parameters for potential form $V(r) = A\exp(-r/\rho) - Cr^{-6}$

Interaction	A (eV)	ρ (Å)	C (eV Å^{-6})
La–O	1644.98	0.36196	0.000
Al–O	1474.40 [1334.31][a]	0.30059	0.000
Mg–O	821.60 [710.50][a]	0.32420	0.000
O–O	22764.20	0.14910	17.890

(b) Shell parameters

Interaction	Shell charge	Spring constant
La(core)–La(shell)	3.000	∞
Al(core)–Al(shell)	3.000	∞
Mg(core)–Mg(shell)	2.000	∞
O(core)–O(shell)	− 2.207	27.29

[a] Values of A in this bracket are appropriate for cations in a tetrahedral site.

2.2. Lattice Energy Calculation

The lattice energy is calculated in the Born model (for a static lattice) by the relation

$$U = 1/2\sum\sum V_{ij}, \quad [4]$$

where the total pairwise interatomic potential, V_{ij}, is given by

$$V_{ij}(r_{ij}) = q_i q_j/r_{ij} + A_{ij}\exp(-r_{ij}/\rho_{ij}) - C_{ij}r_{ij}^{-6}, \quad [5]$$

with the first term representing the Coulombic interactions between species i and j, and the last two the non-Coulombic short range contributions discussed above. The lattice energy is thus calculated exactly, and the only limitations in the procedure arise from a lack of precise knowledge of the interatomic potentials.

Calculations of the crystal energy of the structure under investigation are combined with efficient minimization procedures to determine the equilibrium configuration. A Newton-like second derivation method is used in the energy minimization. In our approach, all the atomic coordinations within the unit cell (not just the symmetry independent ones) are allowed to relax finding the minimum energy configuration. During the atomic coordination relaxation, the lattice vectors are kept fixed. After a minimum energy configuration has been found, the lattice vectors are relaxed using elasticity theory and the calculated residual bulk lattice strains, as described by Cormack (26). The atomic coordinates are then reequilibrated with the new lattice vectors. This procedure is repeated iteratively until all remaining strain (both on the lattice vectors and atomic coordinates) has been removed.

The lattice energy calculation is a static lattice calculation. That is to say, no explicit temperature effects are included; the results refer to 0 K calculations of internal energy. However, it has been shown by Gillan (27) that this is often a good approximation to enthalpies at higher temperatures, since the change in internal energy as the lattice expands is to first order equal to the difference between the enthalpy (which is measured) and the 0 K internal energy. The basis for comparison of our calculated results with experiment lies partly in this observation, but also in the fact that differences in nonconfigurational entropy between structures which have very similar atomic arrangements are expected to be extremely small, especially at room

temperature. This encourages us to ignore entropic effects in structural stability comparison.

2.3. Defect Energy Calculation

Calculations of defect structures and energies introduce one vital feature in addition to those for the perfect lattice methods. This is the occurrence of relaxation of lattice atoms around the defect species. The effect is large because the defect generally provides an extensive perturbation of the surrounding lattice, and, in the case of ionic crystals, the relaxation field is long-range as the perturbation provided by the defect is mainly Coulombic in origin.

The theory of defect energy calculation has been outlined by Catlow *et al.* (28). Basically, the simulation techniques were based on a generalized Mott-Littleton (29) approach developed by Norgett (30), where the important feature is that the crystal surrounding the defect is divided into two regions. The outer region II is treated as a polarizable dielectric continuum, while the atomic coordinates of the distorted inner region I are explicitly relaxed using appropriate interatomic potentials. Therefore, we can write the total energy E of the system as

$$E = E_1(x) + E_2(x, y) + E_3(y), \qquad [6]$$

in which E_1 is the energy of the inner region and thus a function of the coordinates x (and dipole moments) of the ions solely within the region, E_3 depends solely on the displacements y of the ions within region II, and $E_2(x, y)$ is due to interaction of regions I and II.

3. RESULTS AND DISCUSSION

3.1. Site Preference and Distribution of Mg in LMA

The structure of $LaMgAl_{11}O_{19}$ can be derived from that of $SrAl_{12}O_{19}$. Along with the substitution of a divalent Sr ion by a trivalent La ion, the charge compensation is accomplished by replacing an Al ion with an Mg ion. There are five distinct crystallographic Al sites in the aluminate magnetoplumbite structure (see Fig. 1): One trigonal bipyramidal fivefold site (Al(2)), one tetrahedral site (Al(3)), and three octahedral sites (Al(1), Al(4), and Al(5)). The question is: Which Al site does the Mg ion occupy? With the X-ray data for $SrAl_{12}O_{19}$ reported by Lindop *et al.* (31) as the input structure of $LaMgAl_{11}O_{19}$, the equilibrated structures and lattice energies for different Mg ion distributions among the various Al sites were calculated. The lattice energies are listed in Table 2. The lower the lattice energy, the more favorable the configuration of the Mg ion in a structure. It is clearly revealed that the Mg ions prefer to occupy the tetrahedral (Al(3)) sites in MP structure as they do in the spinel structure. This result is in good agreement with the X-ray experimental results (9, 11), as well as that of our earlier simulation study (20), where the site preference of Mg in the MP structure was determined from the substitution energy in $SrAl_{12}O_{19}$. Morgan and Miles (32) suggested that the normal site preferences of cations for tetrahedral or octahedral sites in spinels (33) are presumably paralleled in magnetoplumbite structure also, with the added complexity of competition for, or avoidance of, the nearly trigonal bipyramidal mirror plane sites.

TABLE 2
Effect of Mg Locations on the Lattice Energy per Unit Cell of $LaMgAl_{11}O_{19}$

Model	Mg position	Lattice energy
LMA-I	Mg at Al(3) 4*f* 2, 3	− 1955.17
LMA-II	Mg at Al(3) 4*f* 2, 4	− 1954.91
LMA-III	Mg at Al(3) 4*f* 1, 2	− 1955.45
LMA-IV	Mg at Al(1) 2*a* 1, 2	− 1954.44
LMA-V	Mg at Al(2) 2*b* 1, 2	− 1954.60
LMA-VI	Mg at Al(5) 4*f* 2, 3	− 1950.36
LMA-VII	Mg at Al(5) 4*f* 2, 4	− 1952.38
LMA-VIII	Mg at Al(5) 4*f* 1, 2	− 1952.57
LMA-IX	Mg at Al(4) 12*k* 3, 12	− 1952.86
LMA-X	Mg at Al(4) 12*k* 9, 12	− 1953.45
LMA-XI	Mg at Al(4) 12*k* 6, 12	− 1953.68

Note. Energy units in eV. The position numbers for each equivalent Wyckoff site follow the sequence given for the space group $P6_3/mmc$ in the "International Tables for X-ray Crystallography."

It is also revealed in Table 2 that the distribution of Mg in different tetrahedral sites has some effect on the lattice energy. (Let us recall that only half of the tetrahedral sites are occupied by Mg ions in the structure and that there are three crystallographically distinct distributions of Mg among the tetrahedral sites in a unit cell, resulting in the three models LMA-I, LMA-II, and LMA-III listed in Table 2 (see also Fig. 2).) There is a slight tendency for Mg ions to be separated from each other as far as possible among the tetrahedral sites in the structure. The effect of detailed Mg distribution among the tetrahedral sites on the lattice energy is further investigated with a number of $2\mathbf{a} \times 2\mathbf{a} \times \mathbf{c}$ quadruple supercell models, in which diverse Mg distributions in the tetrahedral sites are taken into account. The supercell models, in which the 8 Mg ions are distributed among the 16 tetrahedral sites as evenly as possible, yield equilibrated lattice energies ranging from −1955.59 to −1955.62 eV per unit cell, slightly lower than that of LMA-III. The tetrahedral site cation distributions in these supercell models have mixed characters of those considered, respectively, in the three basic cell models, LMA-I, II, and III. From the small differences in the lattice energies of the supercell models, we can conclude that in a real compound the Mg (and Al) ions are expected to be randomly distributed in the tetrahedral sites: There will be no enrichment of

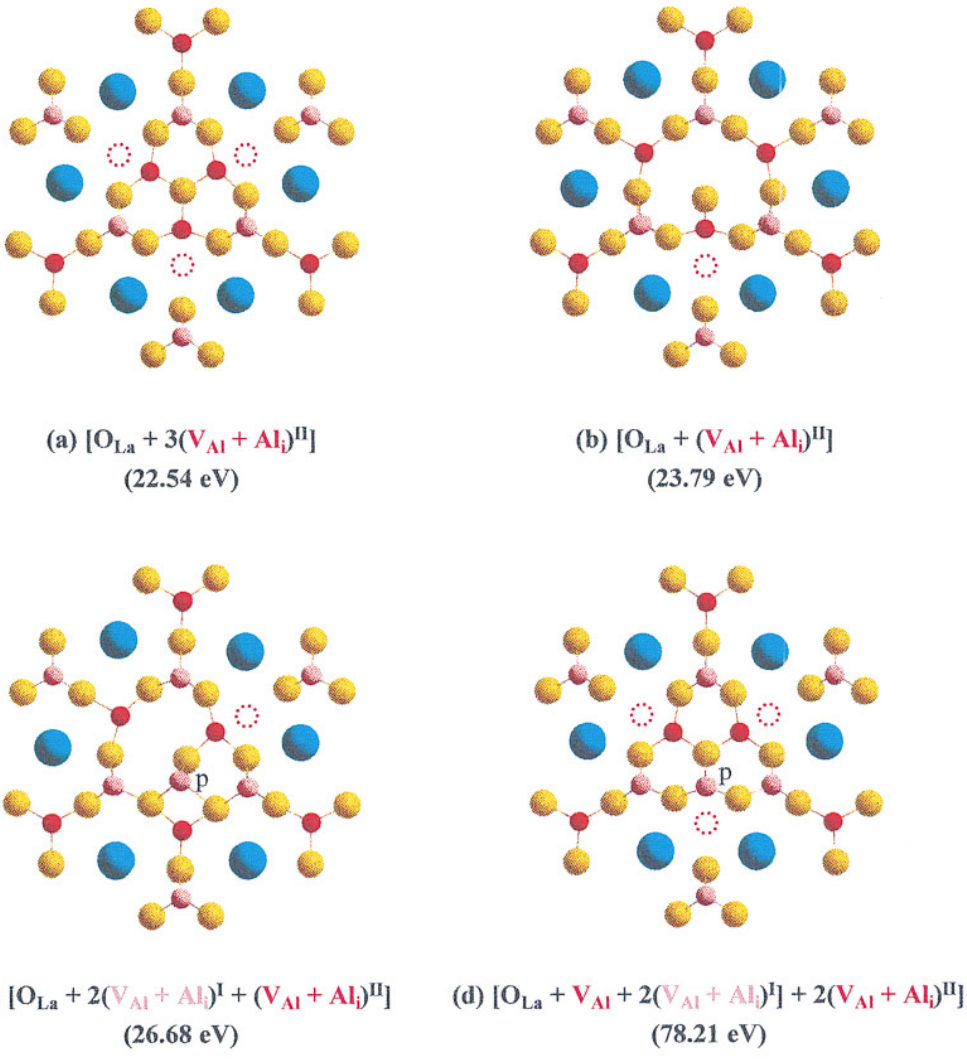

FIG. 4. [001] directional views of the equilibrated mirror plane region structures around defect(s) involving O_{La}. (V_{Al} + Al_i)^{II} denotes the Al(2) Frenkel-like defect occurring in the mirror plane. The others are the same as in Fig. 3. The O_{La} in (b) relaxed to a position near to the first spinel block oxygen layer.

Mg in a particular pair of tetrahedral sites (as in the basic cell models).

3.2. The Effect of Mg Distribution on the Positions of the Al Ion (Al(2)) in LMA

An outstanding controversy in the crystallography of magnetoplumbite structures is whether the cation in the nearly trigonal bipyramidal site, in this case the Al(2) cation, sits on the mirror plane (2*b* site) or is displaced from it along the **c** axis (4*e* site) becoming tetrahedrally coordinated. The structure refinements of $CaAl_{12}O_{19}$ (34, 35), $SrAl_{12}O_{19}$ (31), and $LaMgAl_{11}O_{19}$ (6, 9) indicate that the Al(2) cations are positioned at ideal 2*b* mirror plane sites, whereas those of $LaNiAl_{11}O_{19}$ (36) and $LaFeAl_{11}O_{19}$ (37) reveal that they are displaced from the mirror plane, being positioned in the 4*e* tetrahedral sites. These two types of configurations of the Al(2) cations were referred to as "central atom model" and "split atom model," respectively, by Kimura *et al.* (38). They suggested that the potential around the Al(2) site has double minima in all the magnetoplumbite-type crystals at lower temperatures, and, therefore, there are two plausible states for the Al(2) cations at room temperature, i.e., the static disorder and dynamic disorder states; they also proposed that the split atom model is plausible in $SrAl_{12}O_{19}$ and $SrGa_{12}O_{19}$. However, in our earlier simulation study (39), it was shown that there is no indication of a local potential minimum for the Al(2) cation in a tetrahedral environment in $SrAl_{12}O_{19}$.

The [110] directional views of the three equilibrated unit cell structures, each of which has a distinct Mg distribution among the tetrahedral sites, are shown in Fig. 2. It can be

seen that the Al(2) cation positions are closely related to the detailed distributions of Mg in the spinel blocks: it is revealed that, if two tetrahedral sites, ideally coupled to each other by a mirror plane symmetry, are occupied by Mg ions or by Al ions (as in the half cells of LMA-I), the Al(2) cation is positioned at the ideal mirror plane site, otherwise it is displaced from the mirror plane site.

This structural behavior can be explained mainly by the Coulombic strains imposed on the mirror plane from the tetrahedral sites occupied by either Mg or Al ions: The strains, which are generated when the two tetrahedral sites are occupied by different ions, are relieved by the displacement of the Al(2) ion. Accordingly, the Al(2) ion displaces toward the Mg ion side.

It is worthy of notice that since the **c** axis containing the Al(2) cation includes a triad (ideally $6_3/m$), the cation has six nearest-neighboring Al(3) tetrahedral sites, three in upper and three in lower spinel blocks linked by the cation. Consequently, the position of an Al(2) cation is determined mainly by the Mg and Al distributions in its six nearest-neighboring Al(3) tetrahedral sites. Our calculations for the models generated in a $2\mathbf{a} \times 2\mathbf{a} \times \mathbf{c}$ quadruple supercell, having various cation distributions in the tetrahedral sites, reveal that only when the distribution in the six sites maintains, at least locally, a mirror plane symmetry, the cation sits exactly on the mirror plane.

This result implies that the atomic position (and thus the coordination) in the peculiar trigonal bipyramidal site in MP-type structures is very sensitive to defects, such as vacancies or substitutional aliovalent cations, and their distribution in the neighboring spinel blocks: the atomic position in the site is likely to be determined by the atomic structure in the neighboring spinel blocks. Therefore, it may also be suggested that the relaxation in the trigonal bipyramidal site facilitates the incorporation of the defects in the spinel block.

The displacements of Al(2) from the ideal site in the equilibrated basic cell and supercell models of LMA are calculated to range from zero to 0.26 Å, depending on the detailed Al/Mg configuration in the neighboring tetrahedral sites. The largest displacement, 0.26 Å, is found in LMA-III, where all the upper three sites are occupied by Al ions while all the lower three are occupied by Mg ions. Our results suggest that Al(2) cations in LMA may have both the "central atom" and "split atom" configurations: they are positioned randomly below, above, and on the mirror planes (differing also in the magnitudes of the displacement), according to the diverse cationic configurations in the tetrahedral sites surrounding the Al(2). The experimental observation (6, 9), indicating that LMA has the "central atom" configuration, seems to be reasonable as an averaged approximation, in spite of its inexactness.

On the other hand, based on the displacements of Al(2) in $LaNiAl_{11}O_{19}$ and $LaFeAl_{11}O_{19}$, it can be proposed that Ni and Fe ions behave differently from Mg ions in site preference or distribution in the MP-type structures. Experimentally, the displacements in $LaNiAl_{11}O_{19}$ (36) and $LaFeAl_{11}O_{19}$ (37) were found to be 0.25 and 0.21 Å, respectively. Laville *et al.* (36) suggested, through a single crystal X-ray diffraction study, that the Ni ions are shared between the 4*f* tetrahedral and 2*a* octahedral sites in $LaNiAl_{11}O_{19}$. Our earlier calculation (20) of the substitutional energies in $SrAl_{12}O_{19}$ also indicated that both tetrahedral and octahedral sites are preferred positions for Ni ions to enter.

Consequently, we can propose here that there is no local potential minimum for the Al(2) cation in tetrahedral environment in ideal MP structures (such as $CaAl_{12}O_{19}$), as confirmed also in our earlier simulation work (39), while there may be various local minima in the bipyramidal sites in substitutional derivative MP-types structures (such as $LaMgAl_{11}O_{19}$), depending on the distributions of the spinel block cations.

3.3. Defect Energetics in LMA

Since preliminary defect energy calculations revealed that some defects greatly favor a particular cation distribution in the tetrahedral sites in neighboring spinel blocks, the defect energetics and nonstoichiometry in LMA are investigated through calculations of the formation energies of defects in each of the three equilibrated unit cell structures LMA-I, LMA-II, and LMA-III. Since the differences in lattice energies between the basic cell structures and the quadruple supercell structures are not very great, it was considered adequate to use basic cell structures, instead of the supercell structures, in the calculations of defect energies in LMA.

3.3.1. Intrinsic Disorder

Within the three equilibrated basic cell crystal structures, vacancy and interstitial formation energies are calculated for each of the possible species. The energies are given in Table 3. The lowest formation energies for specific defects among the three structures are rewritten in the last column of the table, as overall defect energies in an LMA crystal in which the three kinds of Mg distributions are mixed.

We can see that the formation energies for the basic atomistic defects (especially, for the interstitial defects) are greatly influenced by the distribution of Mg. In other words, the interstitial defects strongly favor a particular distribution of Mg. For instance, the oxygen interstitial will lead to ordering of Mg (or Al) in the tetrahedral sites around it: Investigation of the detailed structure giving the lowest formation energy reveals that the interstitial oxygen positioned at the center of a spinel block is accompanied with Al ions at the tetrahedral sites in the spinel block and with Mg ions at the tetrahedral sites in the neighboring spinel blocks.

TABLE 3
Calculated Defect Energies for the Basic Atomistic Defects in LMA

Defect	LMA-I	LMA-II	LMA-III	Overall
La vacancy (V_{La})	37.53	38.79	38.89	37.53
La interstitial (La_i)	− 21.72	− 24.09	− 24.76	− 24.76
Al vacancy (V_{Al})	52.87	54.60	54.64	52.87
Al interstitial (Al_i)	− 44.61	− 46.04	− 43.96	− 46.04
Mg vacancy (V_{Mg})	29.47	30.70	29.17	29.17
Mg interstitial (Mg_i)	− 16.83	− 18.60	− 16.28	− 18.60
O vacancy (V_O)	22.21	21.86	23.05	21.86
O interstitial (O_i)	− 15.15	− 17.38	− 13.83	− 17.38
La Frenkel	7.91	7.35	7.07	6.39
Al Frenkel	4.13	4.28	5.34	3.42
Mg Frenkel	6.32	6.05	6.45	5.29
O Frenkel	3.53	2.24	4.61	2.24
Schottky	2.90	3.38	4.04	2.69

Note. Energy units in eV.

The interstitial oxygen at the central spinel block site strongly prefers Al ions rather than Mg ions in its neighboring tetrahedral sites. This may be explained by the tendency to balance the local charge in the structure. This concentrating tendency for Mg ions caused by the defect is found to be greater than the dispersing tendency of Mg ions implied in the perfect lattice energies; while the difference in formation energies of the oxygen interstitial in LMA-II and LMA-III is −3.55 eV per the defect, the difference in lattice energies of the two structures is +0.27 eV per formula unit, $LaMgAl_{11}O_{19}$. Therefore, it is of great importance to consider the three structures for defect energetics in LMA.

The Schottky and Frenkel defect formation energies per constituent defect are determined from the calculated energies for cation and anion vacancies and interstitials. It is noteworthy that because the different types of disorder involve varying numbers of defects, comparison in terms of energy per defect is essential. The thermodynamic grounds for this have been discussed elsewhere (40).

Our calculation results indicate that oxygen Frenkel disorder is the dominant intrinsic defect mode to be expected in LMA. The Schottky disorder, which was suggested by Abrahams *et al.* (9), may also exist, to a somewhat lesser extent.

3.3.2. Probable Defect Processes Involved in Nonstoichiometric LMA

There are a great number of possible nonstoichiometric formulas related to $LaMgAl_{11}O_{19}$. Each formula describes different ways in which the nonstoichiometry may be accommodated. For a particular nonstoichiometric formula, several defect models (and charge compensation mechanisms) are also possible. Since the associated defect processes depend on the energetics of the various defect species concerned, it is worthwhile to calculate the enthalpies of the various reactions for the different formulas of nonstoichiometry to see whether a clear favorite emerged.

Calculated formation energies of some antisite defects, which may be involved in defect processes, are listed in Table 4. It is shown that the formation energy of the cation–cation substitutional defects (A_B) is lower than the sum of the energies of the two basic defects ($A_i + V_B$) constituting the substitutional defects. However, it is found that the formation energies of the defects Al_{La} and La_{Mg} are higher than the energy sums of the equivalent pairs of defects Al_{Mg} and Mg_{La}, and La_{Al} and Al_{Mg}, respectively: The point defects Al_{La} and La_{Mg} are expected to be improbable. Consequently, we consider the subsitutional defects Al_{Mg}, Mg_{Al}, and Mg_{La} (instead of their corresponding basic vacancy–interstitial pairs), and the pairs of defects $Al_{Mg} + Mg_{La}$ (instead of Al_{La}) and $La_{Al} + Al_{Mg}$ (instead of La_{Mg}) in calculations of the enthalpies for the reactions where they are involved.

Mainly based on luminescence data, Stevels (10) proposed that excess oxygen in $La_{1-x}MgAl_{11+5x/3}O_{19+x}$ (this formula is equivalent to the nonstoichiometry involved in the B2 process described below) may be found in "vacant" La sites. In a number of spectroscopic studies on MP-type compounds (10, 16), this "oxygen interstitial at the large cation site" has been postulated to interpret luminescence data. However, our result suggests that the antisite O_{La} defect is improbable, at least, as a simple point defect in LMA, since its formation energy is greater than the sum of the energies of the individual basic defects V_{La} and O_i. The site potential of the La sites (as, indeed, for any cation site) usually precludes occupation of that site by a negatively charged ion, so it is not surprising that a simple O_{La} defect should be energetically unfavorable. This point concerning the O_{La} defect will further be discussed in a later section describing defect complexes.

Equilibrated lattice energies of some oxides which are involved in the defect processes are listed in Table 5.

TABLE 4
Calculated Defect Energies for Substitution

Defect	LMA-I	LMA-II	LMA-III	Overall
Al_{La}	− 9.70	− 12.53	− 9.34	− 12.53
Al_{Mg}	− 29.28	− 29.71	− 29.02	− 29.71
Mg_{Al}	28.64	28.58	29.19	28.58
Mg_{La}	14.75	14.31	15.22	14.31
La_{Al}	18.66	19.48	19.13	18.66
La_{Mg}	− 8.70	− 9.80	− 8.46	− 9.80
O_{La}	22.54	26.68	26.46	22.54

Note. Energy units in eV.

TABLE 5
Equilibrated Lattice Energies per Formula Unit of Some Oxides Involved in the Defect Processes

Compound	Lattice energy
MgO	− 40.44
Al_2O_3	− 158.78
La_2O_3	− 124.14
$LaAlO_3$	− 141.87

Note. Energy units in eV.

The defect processes, each of which may have different reaction paths with respect to the charge compensation mechanisms, are divided into several groups (A to D) and listed along with their reaction enthalpies in Tables 6, 7, 8, and 9. The charge compensation mechanisms in the reactions are implicitly represented in the defect energy expressions given in the tables.

The defect processes, in which each cation deficiency is exactly compensated by oxygen deficiency, are gathered into group A in Table 6. The high reaction energies imply that these processes are not likely to occur. The nonstoichiometric formula $LaMg_{1-x}Al_{11}O_{19-x}$ involved in the A3 process can be expressed also as $LaMg_yAl_{11}O_{18+y}$. This latter formula was used as initial compositions ($0 < y < 1$) for a series of lanthanum hexaaluminates containing diverse divalent cations, by Gasperin *et al.* (11), in order to understand the role played by M^{2+} ions in the formation of LMA-type structures. Their structural refinement revealed that the stoichiometries of their grown crystals did not follow the nonstoichiometric formula. They suggested that in all these nonstoichiometric phases, the charge compensation mechanism would be very complicated, since in most of them the vacancies and interstitial atoms could be found simultaneously. Our simulated reaction enthalpy of the defect process A3 clearly indicates that the nonstoichiometry $LaMg_yAl_{11}O_{18+y}$ is improbable.

The defect processes group B in Table 7 concern the various nonstoichiometries which are possible when Al ions are incorporated in excess into the ideal LMA structure. It is noteworthy that since the reactants in all of the processes are the same, the reaction enthalpies can be thought to be normalized and thus be directly compared with one another.

Among the various Al-excess defect processes, we can see that the processes B4b, B5, B6, B7, B8c, B9b, and B11b are likely to occur, from the viewpoint of reaction enthalpies, even though the degrees of nonstoichiometry at equilibrium will be different and are expected to be most significant in the two processes B4b and B6. Therefore, the reaction path for these Al-excess processes is expected to be various and will be determined by kinetics or by experimental conditions, such as starting composition and homogeneity of mixing. It is important to note that all these promising Al-excess defect processes involve the Al_{Mg} defect: It is evident in the reaction enthalpies that this defect plays a key role in the Al excess nonstoichiometric processes in LMA. The compensating defect species for the Al_{Mg} are expected to be O_i, V_{Al}, V_{La}, or the combinations of them.

On the other hand, among these promising Al-excess defect processes, the processes B6, B7, B8, and B9 give rise to oxygen-excess nonstoichiometries. The excess oxygen in these processes is positioned as an O_i at the center of the spinel block whose tetrahedral sites are occupied by Al ions only, as mentioned in Section 3.3.1.

The defect processes group C in Table 8 concern the various nonstoichiometries which are possible when Mg ions are incorporated in excess into the ideal LMA structure. Among these Mg-excess defect processes, the process C5c is found to be energetically most favorable. The processes C4 is also likely to occur. It is noteworthy that the defect Mg_{Al} plays an important part in the Mg-excess defect processes, as the Al_{Mg} does in the Al-excess processes. The compensating defect for the Mg_{Al} is expected to be Mg_i or V_O, which may be determined by experimental conditions.

The defect processes group D in Table 9 concern the nonstoichiometries which are possible when La ions are incorporated in excess into the ideal LMA structure. It is revealed that the process D1, in which La ions replace Al ions, is most preferred energetically among the La-excess processes. However, this La-excess defect process is energetically less favored than the Al- or Mg-excess processes discussed above.

Consequently, the probable nonstoichiometries in LMA are those involved in the defect processes B4, B5, B6, B7, B8, B9, B11, C4, and C5: $LaMg_{1-3x/2}Al_{11+x}O_{19}$, $La_{1-x/3}Mg_{1-x}Al_{11+x}O_{19}$, $LaMg_{1-x}Al_{11+x}O_{19+x/2}$, $La_{1-x/5}Mg_{1-x}Al_{11+x}O_{19+x/5}$, $La_{1-x/3}Mg_{1-2x/3}Al_{11+x}O_{19+x/3}$, $La_{1-x/7}Mg_{1-8x/7}Al_{11+x}O_{19+x/7}$, $La_{1-x/5}Mg_{1-6x/5}Al_{11+x}O_{19}$, $La_{1-x/5}Mg_{1-x}Al_{11+x}O_{19+x/5}$, $LaMg_{1+x}Al_{11-x}O_{19-x/2}$, and $LaMg_{1+x}Al_{11-2x/3}O_{19}$. The preference for each of these formulas will depend on the kinetics and experimental conditions.

TABLE 6
Calculated Enthalpies for Defect Processes, where Cation Deficiency is Compensated by Oxygen Deficiency

A1. $LaMgAl_{11}O_{19} \rightarrow La_{1-x}MgAl_{11}O_{19-3x/2} + (x/2)La_2O_3$
$E_{A1} = E(V_{La}) + (3/2)E(V_O) + (1/2)E_{lat}(La_2O_3) = 8.25$ eV

A2. $LaMgAl_{11}O_{19} \rightarrow LaMgAl_{11-x}O_{19-3x/2} + (x/2)Al_2O_3$
$E_{A2} = E(V_{Al}) + (3/2)E(V_O) + (1/2)E_{lat}(Al_2O_3) = 6.27$ eV

A3. $LaMgAl_{11}O_{19} \rightarrow LaMg_{1-x}Al_{11}O_{19-x} + xMgO$
$E_{A3} = E(V_{Mg}) + E(V_O) + E_{lat}(MgO) = 10.60$ eV

TABLE 7
Al-Excess Defect Processes in LMA and Their Calculated Enthalpies

B1. $LaMgAl_{11}O_{19} + (x/2)Al_2O_3 \rightarrow LaMgAl_{11+x}O_{19+3x/2}$
$E_{B1a} = E(Al_i) + (3/2)E(O_i) - (1/2)E_{lat}(Al_2O_3) = 7.27$ eV
$E_{B1b} = E(Al_{Mg}) + E(Mg_i) + (3/2)E(O_i) - (1/2)E_{lat}(Al_2O_3) = 5.00$ eV

B2. $LaMgAl_{11}O_{19} + (x/2)Al_2O_3 \rightarrow La_{1-3x/5}MgAl_{11+x}O_{19+3x/5} + (3x/10)La_2O_3$
$E_{B2a} = E(Al_i) + (3/5)E(O_i) + (3/5)E(V_{La}) + (3/10)E_{lat}(La_2O_3) - (1/2)E_{lat}(Al_2O_3) = 8.20$ eV
$E_{B2b} = E(Al_{Mg}) + E(Mg_{La}) + (2/5)E(La_i) + (3/5)E(O_i) + (3/10)E_{lat}(La_2O_3) - (1/2)E_{lat}(Al_2O_3) = 6.42$ eV
$E_{B2c} = (7/5)E(Al_{Mg}) + E(Mg_{La}) + (2/5)E(La_{Al}) + (2/5)E(Mg_i) + (3/5)E(O_i) + (3/10)E_{lat}(La_2O_3) - (1/2)E_{lat}(Al_2O_3) = 4.46$ eV

B3. $LaMgAl_{11}O_{19} + (x/2)Al_2O_3 \rightarrow La_{1-x}MgAl_{11+x}O_{19} + (x/2)La_2O_3$
$E_{B3} = E(Al_{Mg}) + E(Mg_{La}) + (1/2)E_{lat}(La_2O_3) - (1/2)E_{lat}(Al_2O_3) = 1.92$ eV

B4. $LaMgAl_{11}O_{19} + (x/2)Al_2O_3 \rightarrow LaMg_{1-3x/2}Al_{11+x}O_{19} + (3x/2)MgO$
$E_{B4a} = E(Al_{Mg}) + (1/2)E(V_{Mg}) + (3/2)E_{lat}(MgO) - (1/2)E_{lat}(Al_2O_3) = 3.61$ eV
$E_{B4b} = (3/2)E(Al_{Mg}) + (1/2)E(V_{Al}) + (3/2)E_{lat}(MgO) - (1/2)E_{lat}(Al_2O_3) = 0.60$ eV

B5. $LaMgAl_{11}O_{19} + (x/2)Al_2O_3 \rightarrow La_{1-x/3}Mg_{1-x}Al_{11+x}O_{19} + (x/6)La_2O_3 + xMgO$
$E_{B5} = E(Al_{Mg}) + (1/3)E(V_{La}) + (1/6)E_{lat}(La_2O_3) + E_{lat}(MgO) - (1/2)E_{lat}(Al_2O_3) = 1.06$ eV

B6. $LaMgAl_{11}O_{19} + (x/2)Al_2O_3 \rightarrow LaMg_{1-x}Al_{11+x}O_{19+x/2} + xMgO$
$E_{B6} = E(Al_{Mg}) + (1/2)E(O_i) + E_{lat}(MgO) - (1/2)E_{lat}(Al_2O_3) = 0.55$ eV

B7. $LaMgAl_{11}O_{19} + (x/2)Al_2O_3 \rightarrow La_{1-x/5}Mg_{1-x}Al_{11+x}O_{19+x/5} + (x/10)La_2O_3 + xMgO$
$E_{B7} = E(Al_{Mg}) + (1/5)E(O_i) + (1/5)E(V_{La}) + (1/10)E_{lat}(La_2O_3) + E_{lat}(MgO) - (1/2)E_{lat}(Al_2O_3) = 0.86$ eV

B8. $LaMgAl_{11}O_{19} + (x/2)Al_2O_3 \rightarrow La_{1-x/3}Mg_{1-2x/3}Al_{11+x}O_{19+x/3} + (x/6)La_2O_3 + (2x/3)MgO$
$E_{B8a} = (1/3)E(V_{La}) + (1/3)E(O_i) + E(Al_i) + (2/3)E(V_{Mg}) + (1/6)E_{lat}(La_2O_3) + (2/3)E_{lat}(MgO) - (1/2)E_{lat}(Al_2O_3) = 11.86$ eV
$E_{B8b} = (1/3)E(V_{La}) + (1/3)E(O_i) + (1/3)E(Al_i) + (2/3)E(Al_{Mg}) + (1/6)E_{lat}(La_2O_3) + (2/3)E_{lat}(MgO) - (1/2)E_{lat}(Al_2O_3) = 3.30$ eV
$E_{B8c} = E(Al_{Mg}) + (1/3)E(Mg_{La}) + (1/3)E(O_i) + (1/6)E_{lat}(La_2O_3) + (2/3)E_{lat}(MgO) - (1/2)E_{lat}(Al_2O_3) = 1.01$ eV

B9. $LaMgAl_{11}O_{19} + (x/2)Al_2O_3 \rightarrow La_{1-x/7}Mg_{1-8x/7}Al_{11+x}O_{19+x/7} + (x/14)La_2O_3 + (8x/7)MgO$
$E_{B9a} = (1/7)E(V_{La}) + (1/7)E(O_i) + E(Al_{Mg}) + (1/7)E(V_{Mg}) + (1/14)E_{lat}(La_2O_3) + (8/7)E_{lat}(MgO) - (1/2)E_{lat}(Al_2O_3) = 1.64$ eV
$E_{B9b} = (1/7)E(V_{La}) + (1/7)E(O_i) + (8/7)E(Al_{Mg}) + (1/7)E(V_{Al}) + (1/14)E_{lat}(La_2O_3) + (8/7)E_{lat}(MgO) - (1/2)E_{lat}(Al_2O_3) = 0.78$ eV

B10. $LaMgAl_{11}O_{19} + (x/2)Al_2O_3 \rightarrow La_{1-x}Mg_{1-x}Al_{11+x}O_{19-x} + (x/2)La_2O_3 + xMgO$
$E_{B10} = E(V_{La}) + E(Al_{Mg}) + E(V_O) + (1/2)E_{lat}(La_2O_3) + E_{lat}(MgO) - (1/2)E_{lat}(Al_2O_3) = 6.56$ eV

B11. $LaMgAl_{11}O_{19} + (x/2)Al_2O_3 \rightarrow La_{1-x/5}Mg_{1-6x/5}Al_{11+x}O_{19} + (x/10)La_2O_3 + (6x/5)MgO$
$E_{B11a} = (1/5)E(V_{La}) + E(Al_{Mg}) + (1/5)E(V_{Mg}) + (1/10)E_{lat}(La_2O_3) + (6/5)E_{lat}(MgO) - (1/2)E_{lat}(Al_2O_3) = 2.08$ eV
$E_{B11b} = (1/5)E(V_{La}) + (6/5)E(Al_{Mg}) + (1/5)E(V_{Al}) + (1/10)E_{lat}(La_2O_3) + (6/5)E_{lat}(MgO) - (1/2)E_{lat}(Al_2O_3) = 0.88$ eV

B12. $LaMgAl_{11}O_{19} + (x/2)Al_2O_3 \rightarrow La_{1-x}Mg_{1-2x}Al_{11+x}O_{19-2x} + (x/2)La_2O_3 + 2xMgO$
$E_{B12a} = E(V_{La}) + E(Al_{Mg}) + E(V_{Mg}) + 2E(V_O) + (1/2)E_{lat}(La_2O_3) + 2E_{lat}(MgO) - (1/2)E_{lat}(Al_2O_3) = 17.15$ eV
$E_{B12b} = E(V_{La}) + 2E(Al_{Mg}) + E(V_{Al}) + 2E(V_O) + (1/2)E_{lat}(La_2O_3) + 2E_{lat}(MgO) - (1/2)E_{lat}(Al_2O_3) = 11.14$ eV

3.3.3. Defect Complexes

In order to explain the nonstoichiometry in lanthanum hexaaluminate (LHA, ideal composition $LaAl_{11}O_{18}$), Iyi *et al.* (13) proposed two types of defect models, a "vacancy model" and an "interstitial oxygen model," based on the MP structure. They also postulated two types of defect configuration, "type 1" and "type 2," for each model. In the type 1 vacancy model, the defect complex is composed of a lanthanum vacancy (V_{La}) and an aluminum interstitial (Al_i) migrated from a spinel block 12*k* site to mirror plane region according to Frenkel defect mechanism; the Al(2) cation on the mirror plane 2*b* site, adjacent to the Al_i, relaxed to a 4*e* tetrahedral site. In the type 2 configuration, the complex is composed of a pair of cation vacancies, V_{La} and V_{Al}, on the mirror plane and a pair of aluminum Frenkel defects formed just above and below the center of the vacancy pair. On the other hand, in the interstitial oxygen model, which is conceptually identical to the model proposed by Stevels (10, 16), the vacant La site of the defect complex in the vacancy model is occupied by an interstitial oxygen (O_{La}). Our recent simulation study on LHA (17) clearly reveals that the vacancy model is energetically favored over the interstitial oxygen model and also that the

TABLE 8
Mg-Excess Defect Processes in LMA and Their Calculated Enthalpies

C1. $LaMgAl_{11}O_{19} + xMgO \rightarrow La_{1-x}Mg_{1+x}Al_{11}O_{19-x/2} + (x/2)La_2O_3$
$E_{C1} = E(Mg_{La}) + (1/2)E(V_O) + (1/2)E_{lat}(La_2O_3) - E_{lat}(MgO) = 3.62$ eV

C2. $LaMgAl_{11}O_{19} + xMgO \rightarrow La_{1-2x/3}Mg_{1+x}Al_{11}O_{19} + (x/3)La_2O_3$
$E_{C2a} = E(Mg_i) + (2/3)E(V_{La}) + (1/3)E_{lat}(La_2O_3) - E_{lat}(MgO) = 5.48$ eV
$E_{C2b} = E(Mg_{La}) + (1/3)E(La_i) + (1/3)E_{lat}(La_2O_3) - E_{lat}(MgO) = 5.12$ eV
$E_{C2c} = E(Mg_{La}) + (1/3)E(La_{Al}) + (1/3)E(Al_{Mg}) + (1/3)E(Mg_i) + (1/3)E_{lat}(La_2O_3) - E_{lat}(MgO) = 3.49$ eV
$E_{C2d} = (2/3)E(Mg_{La}) + (1/3)E(Mg_i) + (1/3)E_{lat}(La_2O_3) - E_{lat}(MgO) = 2.40$ eV

C3. $LaMgAl_{11}O_{19} + xMgO \rightarrow La_{1-2x/5}Mg_{1+x}Al_{11}O_{19+2x/5} + (x/5)La_2O_3$
$E_{C3a} = E(Mg_i) + (2/5)E(V_{La}) + (2/5)E(O_i) + (1/5)E_{lat}(La_2O_3) - E_{lat}(MgO) = 5.07$ eV
$E_{C3b} = E(Mg_{La}) + (3/5)E(La_i) + (2/5)E(O_i) + (1/5)E_{lat}(La_2O_3) - E_{lat}(MgO) = 8.11$ eV
$E_{C3c} = E(Mg_{La}) + (3/5)E(La_{Al}) + (3/5)E(Al_{Mg}) + (3/5)E(Mg_i) + (2/5)E(O_i) + (1/5)E_{lat}(La_2O_3) - E_{lat}(MgO) = 5.18$ eV

C4. $LaMgAl_{11}O_{19} + xMgO \rightarrow LaMg_{1+x}Al_{11-x}O_{19-x/2} + (x/2)Al_2O_3$
$E_{C4} = E(Mg_{Al}) + (1/2)E(V_O) + (1/2)E_{lat}(Al_2O_3) - E_{lat}(MgO) = 0.56$ eV

C5. $LaMgAl_{11}O_{19} + xMgO \rightarrow LaMg_{1+x}Al_{11-2x/3}O_{19} + (x/3)Al_2O_3$
$E_{C5a} = E(Mg_i) + (2/3)E(V_{Al}) + (1/3)E_{lat}(Al_2O_3) - E_{lat}(MgO) = 4.16$ eV
$E_{C5b} = E(Mg_{Al}) + (1/3)E(Al_i) + (1/3)E_{lat}(Al_2O_3) - E_{lat}(MgO) = 0.75$ eV
$E_{C5c} = (2/3)E(Mg_{Al}) + (1/3)E(Mg_i) + (1/3)E_{lat}(Al_2O_3) - E_{lat}(MgO) = 0.37$ eV

C6. $LaMgAl_{11}O_{19} + xMgO \rightarrow LaMg_{1+x}Al_{11-2x/5}O_{19+2x/5} + (x/5)Al_2O_3$
$E_{C6a} = E(Mg_i) + (2/5)E(V_{Al}) + (2/5)E(O_i) + (1/5)E_{lat}(Al_2O_3) - E_{lat}(MgO) = 4.28$ eV
$E_{C6b} = E(Mg_{Al}) + (3/5)E(Al_i) + (2/5)E(O_i) + (1/5)E_{lat}(Al_2O_3) - E_{lat}(MgO) = 2.69$ eV
$E_{C6c} = (2/5)E(Mg_{Al}) + (3/5)E(Mg_i) + (2/5)E(O_i) + (1/5)E_{lat}(Al_2O_3) - E_{lat}(MgO) = 2.01$ eV

defect complex configuration should be the type 2, confirming Iyi *et al.*'s conclusions made without definite evidence.

In this section, we focus our attention on the possibilities for such defect complexes to form in the interspinel mirror plane layer in LMA, which is different in composition from LHA. It is worthy to point out that LMA contains both Mg and Al ions in its spinel block, while LHA contains Al ions only. As discussed later, this approach gives us an insight into the role of divalent cations such as Mg in the stabilization of the MP structure in various lanthanide-containing hexaaluminates.

A number of possible defect complexes have been examined. Formation energies and equilibrated configurations of the defect complexes are also dependent on the distribution of Mg (and Al) ions among the spinel block tetrahedral sites. In the three perfect lattice structures, LMA-I, LMA-II, and LMA-III, on which defect calculations are based, there are four types of mirror planes in conjunction with the spinel block cation distribution (see Fig. 2): The lower and upper mirror planes in LMA-I and the mirror planes in LMA-II and LMA-III. Hence, these four types of interspinel layers are considered individually in the calculations. The equilibrated configurations which yield lowest formation energies for a particular defect complex among the four layers are described in general.

3.3.3.1. Defect complexes involving V_{La}. The equilibrated structure around a simple point defect V_{La} has the

TABLE 9
La-Excess Defect Processes in LMA and Their Calculated Enthalpies

D1. $LaMgAl_{11}O_{19} + (x/2)La_2O_3 \rightarrow La_{1+x}MgAl_{11-x}O_{19} + (x/2)Al_2O_3$
$E_{D1} = E(La_{Al}) + (1/2)E_{lat}(Al_2O_3) - (1/2)E_{lat}(La_2O_3) = 1.34$ eV

D2. $LaMgAl_{11}O_{19} + (x/2)La_2O_3 \rightarrow La_{1+x}Mg_{1-3x/2}Al_{11}O_{19} + (3x/2)MgO$
$E_{D2a} = E(La_{Al}) + E(Al_{Mg}) + (1/2)E(V_{Mg}) + (3/2)E_{lat}(MgO) - (1/2)E_{lat}(La_2O_3) = 4.95$ eV
$E_{D2b} = E(La_{Al}) + E(Al_{Mg}) + (1/2)E(O_i) + E_{lat}(MgO) - (1/2)E_{lat}(La_2O_3) = 1.89$ eV

D3. $LaMgAl_{11}O_{19} + (x/2)La_2O_3 \rightarrow La_{1+x}MgAl_{11}O_{19+3x/2}$
$E_{D3a} = E(La_i) + (3/2)E(O_i) - (1/2)E_{lat}(La_2O_3) = 11.24$ eV
$E_{D3b} = E(La_{Al}) + E(Al_{Mg}) + E(Mg_i) + (3/2)E(O_i) - (1/2)E_{lat}(La_2O_3) = 6.35$ eV

configuration shown in Fig. 3a. In order to check the possibility of the defect complexes postulated by Iyi *et al.* (13), the formation of the aluminum Frenkel-like defects near the V_{La} is taken into account. When a single Al Frenkel defect, an Al ion shifts from the spinel block 12*k* site to the mirror plane region 12*k* site, is initially introduced, the configuration shown in Fig. 3b results: The initial structure is almost maintained. This defect complex configuration is the same as the "type 1" configuration postulated by Iyi *et al.* (13); the Al(2) ion on the 2*b* site, adjacent to the interstitial aluminum ion of the Frenkel-like defect, relaxed to the 4*e* tetrahedral site. (This relaxation does not come into view in the figure.) This configuration was also obtained even when the Al Frenkel defects are initially introduced in a pair: The input Al_i of the second Al Frenkel defect naturally relaxed to the original spinel block site. However, it is found that this "type 1" defect complex is not favored energetically, as in pure LHA: The lowest formation energy of this defect complex $[V_{La} + (V_{Al} + Al_i)]$ is 38.80 eV, which is greater than that of the simple point defect $[V_{La}]$, 37.53 eV.

When the lanthanum vacancy is coupled with an aluminum vacancy in a neighboring 2*b* site forming a vacancy pair, V_{La} and V_{Al}, in the mirror plane, the defect complex configuration shown in Fig. 3c results: A *single* Al Frenkel-like defect is formed just below (or above) the center of the vacancy pair. It is also revealed that the Al Frenkel-like defect cannot be formed in a pair both above and below the center, as in the previous case. However, the defect complex $[V_{La} + V_{Al} + (V_{Al} + Al_i)]$ of the Fig. 3c configuration is not bound, since the sum of the formation energies (90.40 eV) of the isolated point defects V_{La} and V_{Al} is much smaller than the formation energy (94.41 eV) of the complex.

However, when all the tetrahedral sites in the neighboring spinel blocks of the vacancy pair (V_{La} and V_{Al}) are occupied by Al ions, through the substitution of the Mg ions with Al ions, the Al Frenkel-like defects are naturally formed in a pair just above and below the center of the vacancy pair, as shown in Fig. 3d, where the two Al_i's overlap in the view. (It is noteworthy that Fig. 3c contains a single Al_i while Fig. 3d does two (a pair).) This mirror plane region defect configuration was postulated as "type 2" and adopted for the defect structure in LHA by Iyi *et al.* (13). Accompanied with the substitutional Al_{Mg} defects in its surrounding tetrahedral shell, this "type 2" configuration turns out to be favored energetically in the mirror plane region of LMA. The formation energy of the defect complex $[V_{La} + V_{Al} + 2(V_{Al} + Al_i) + 6Al_{Mg}]$, maintaining the charge neutrality by itself, is calculated to be -88.01 eV, while the sum of the energies $([V_{La}] + [V_{Al}] + 6[Al_{Mg}])$ of individual point defects is -87.86 eV.

This result implies that, when the spinel block tetrahedral sites are occupied by Al ions (as in LHA), the spinel block 12*k* site Al ions will relax naturally toward the vacancy pair (V_{La} and V_{Al}) to compensate the local effective negative charges in the vacancy region, and there is a tendency to form a defect complex of type 2. (It is noteworthy, therefore, that the enthalpy of the defect process B11 in Table 7 can have a slightly lower value (0.85 eV) with the formation of the defect complex $[V_{La} + V_{Al} + 2(V_{Al} + Al_i) + 6Al_{Mg}]$ than the 0.88 eV calculated with the point defect energies.) On the other hand, when the tetrahedral sites are occupied in part by Mg ions (as in LMA), the formation of the defect complex is unfavored. This structural behavior in LMA can be explained with the fact that the Mg ions exert less Coulombic strains than the Al ions, on the spinel block 12*k* site Al ions which must relax to the mirror plane region in order to form the defect complex. Here lies a role played by divalent cations such as Mg in the stabilization of the MP-type structures of lanthanide hexaaluminates: Mg ions, located in the spinel block tetrahedral sites, suppress the formation of cation vacancies in the mirror plane, through hindering the relaxation of the 12*k* Al ions by which the vacancies are stabilized. In other words, Mg ions stabilize the spinel block and hence the mirror plane.

It has been reported that LMA type compounds suffered a loss of divalent cations during crystal growth, leading to a significant departure from their starting compositions (2, 11, 37, 41, 42). It was also found that the smaller the content of M^{2+}, the higher the disorder in the crystal lattice, the worse the crystal growth, and the more intense the diffuse scattering in (001) planes (11).

In highly M^{2+}-deficient LMA-type compounds, the type 2 vacancy model defect complex, $[V_{La} + V_{Al} + 2(V_{Al} + Al_i)]$, is expected to be formed in their interspinel mirror plane region whose neighboring tetrahedral 4*f* sites are occupied fully (or mainly) by Al ions. In other words, high deficiency in M^{2+} content would lead to the formation of the defect complex, resulting in La and Al deficiency in the interspinel mirror plane; the concentration of the defect complex would be related to the degree of nonstoichiometry. In addition, the formation of the defect complex is accompanied by lattice relaxation around it: For instance, as can be seen in Fig. 3d, the La ions adjacent to the defect complex displaced from their ideal 2*d* sites to 6*h* sites.

The partial occupancy of La and Al(2) sites and displacement of the ions of the mirror plane in Mg-deficient LMA, which result from the formation of the defect complex, may be the origins of the diffuse scattering in the **ab** planes. The two-dimensional diffuse scattering found in defective LMA-type compounds is thought to have originated from either ordering between vacant and occupied sites of La ions within the mirror plane or correlation between positional shifts of these ions (43).

It is worthy of notice that our simulation study suggests that maintaining stoichiometric content of divalent cation during crystal growth of LMA-type compounds would be crucial to reduce lattice disorder and obtain high quality single crystals.

3.3.3.2. Defect complexes involving O_{La}. The equilibrated structure around the point defect O_{La} is shown in Fig. 4a. It forms a defect complex rather than remaining as a simple point defect: The three Al(2) ions neighboring the O_{La} relax naturally to 6*h* sites from the ideal 2*b* sites in the mirror plane. The relaxation of the Al(2) ions may be considered as Al Frenkel-like defects occurring triply in the mirror plane. However, as discussed in Section 3.3.2, the formation energy 22.54 eV of this defect complex (i.e., O_{La} in the previous discussion) is greater than the sum of the energies, 20.15 eV, of the individual point defects V_{La} and O_i, indicating the instability of this antisite defect O_{La}.

When we consider initially the formation of various Al Frenkel defects around the O_{La}, a number of distinct defect complex configurations result as illustrated typically in Fig. 4b to 4d, where their formation energies are also given in parentheses. None of the various configurations has lower formation energy than the Fig. 4a configuration, setting aside the individual point defects. This is somewhat different from our simulation results on LHA (17), where it was found that Fig. 4c-type configuration was most favored (rather than Fig. 4a type) in the pure LHA system. This different structural behavior is closely related to the role of Mg ions, as discussed above. The local effective negative charges due to the O_{La} seem to be efficiently relieved in LMA by the relaxation of the Al(2) ions in the mirror plane (Fig. 4a), rather than by that of the 12*k* Al ions, due to the presence of Mg ions, while both types of relaxation are likely to be involved in the case of LHA. However, in spite of this type of difference, it was also indicated in the results (17) that the oxygen interstitial in LHA does not prefer the vacant La site but the central spinel block site, consistent with the present result for LMA.

The situation was not changed when the O_{La} is combined with an aluminum vacancy in a neighboring 2*b* mirror plane site, forming a defect pair, O_{La} and V_{Al}, in the mirror plane. The lowest energy configuration of the defect complex including this defect pair is shown in Fig. 4d. Four Al Frenkel-like defects were generated around the defect pair: two in the mirror planes and the other two from the spinel blocks. The formation energy of this complex $[O_{La} + V_{Al} + 4(V_{Al} + Al_i)]$ is 78.21 eV, which is much greater than the sum of the energies, 73.02 eV, of the individual point defects, V_{La}, O_i, and V_{Al}, indicating the instability of this complex.

Consequently, we may conclude that the O_{La} antisite defect is improbable not only as a simple point defect but also as a member of a defect complex, in contrast to our earlier conclusion (18) supporting the feasibility of the O_{La} forming defect complexes in the mirror plane region. Our present simulation results suggest that the postulation of the oxygen interstitial at the large cation site, which has been proposed to interpret luminescence data in some MP-type structures, seems to be inappropriate. There may be a different mechanism (rather than the interaction between the O_{La} and active ions) to yield the luminescent properties of the active ions, as discussed by Viana *et al.* (2).

4. CONCLUSIONS

Computer-based atomistic simulation methods are applied to address quantitatively the defect energetics and crystal chemistry of LMA. The tetrahedral site preference of Mg in the magnetoplumbite structure is determined by calculating lattice energies for different Mg ion distributions. The position of trigonal bipyramidal Al(2) cations can be displaced from the ideal mirror plane site along the **c** axis and can be positioned on the ideal site, depending on the detailed Mg distributions among the tetrahedral sites in the neighboring spinel blocks.

It is revealed that the intrinsic and extrinsic disorders in LMA are much influenced by the distribution of Mg among the tetrahedral sites in the structure. Our calculations show that oxygen Frenkel disorder is the dominant defect mode to be expected, even though the Schottky disorder may also exist. Several feasible defect processes in nonstoichiometric LMA are determined from the enthalpies of the quasi-chemical reactions for the processes with simple point defect energies. It is revealed that the defects Al_{Mg} and Mg_{Al} play a key role in the Al-excess and Mg-excess processes, respectively.

In addition, we have also modeled some defect complexes in the mirror plane regions. Our results indicate that, in the stoichiometric LMA, the "type 1" and "type 2" defect complexes, which were postulated by Iyi *et al.* (13) to explain the nonstoichiometry in pure LHA, are not likely to be formed. In Mg-deficient (and Al-excess) nonstoichiometric LMA, however, it is suggested that the type 2 vacancy model defect complex is expected to be formed in the interspinel layers. We can conclude that Mg ions, positioned in the spinel block tetrahedral sites, suppress the relaxation of the 12*k* Al ions, by which cation vacancies in the mirror plane are stabilized through forming the defect complex. Our calculations also revealed that the O_{La} defect is improbable in LMA not only as a simple point defect but also as a member of a defect complex.

ACKNOWLEDGMENTS

The U.S. Department of Energy, Office of Basic Energy Sciences is thanked for financial support under Grant DE-FG02-91ER45451. Some of the calculations reported here were performed at the Cornell Theory Center, which is funded in part by New York State, the National Science Foundation and IBM corporation.

REFERENCES

1. L. D. Schearer, M. Leduc, D. Vivien, A. M. Lejus, and J. Thery, *IEEE J. Quantum Electron.* **QE-22,** 713 (1986).

2. B. Viana, G. Aka, D. Vivien, A. M. Lejus, J. Thery, A. Derory, J. C. Bernier, C. Garapon, and G. Boulon, *J. Appl. Phys.* **64,** 1398 (1988).
3. B. Martinat, D. Gourier, A. M. Lejus, and D. Vivien, *J. Solid State Chem.* **89,** 147 (1990).
4. R. Collongues and D. Vivien, *J. Solid State Chem.* **96,** 97 (1992).
5. S. I. Balabaev, B. V. Ignatev, O. V. Kuzmin, V. A. Lebedev, V. F. Pisarenko, and Yu. M. Chuev, *Opt. Spectrosc.* (*Engl. Transl.*) **70,** 364 (1991).
6. A. Kahn, A. M. Lejus, M. Madsac, J. Thery, D. Vivien, and J. C. Bernier, *J. Appl. Phys.* **52,** 6864 (1981).
7. V. Adelskold, *Ark. Kemi. Mineral. Geol. A* **12,** 1 (1938).
8. J. M. P. J. Verstegen, *J. Electrochem. Soc.* **121,** 1623 (1974).
9. S. C. Abrahams, P. Marsh, and C. D. Brandle, *J. Chem. Phys.* **86,** 4221 (1987).
10. A. L. N. Stevels, *J. Electrochem. Soc.* **125,** 588 (1978).
11. M. Gasperin, M. C. Saine, A. Kahn, F. Laville, and A. M. Lejus, *J. Solid State Chem.* **54,** 61 (1984).
12. R. S. Roth and S. Hasko, *J. Am. Ceram. Soc.* **41,** 146 (1958).
13. N. Iyi, Z. Inoue, S. Takekawa, and S. Kimura, *J. Solid State Chem.* **54,** 70 (1984).
14. C. Brisi, F. Abbattista, and M. Vallino, *Rev. Int. Hautes Temp. Refract.* **17,** 331 (1980).
15. A. L. N. Stevels and J. M. P. J. Verstegen, *J. Lumin.* **14,** 207 (1976).
16. A. L. N. Stevels, *J. Lumin.* **17,** 121 (1978); *J. Lumin.* **20,** 99 (1979).
17. J.-G. Park and A. N. Cormack, *J. Solid State Chem.*, in press.
18. L. Xie and A. N. Cormack, *J. Solid State Chem.* **88,** 543 (1990).
19. J.-G. Park and A. N. Cormack, *Philos. Mag. B* **73,** 21 (1996).
20. L. Xie and A. N. Cormack, *Mater. Lett.* **9,** 474 (1990).
21. L. Xie, Ph.D. Thesis, Alfred University, Alfred, New York, 1990.
22. B. G. Dick and A. W. Overhauser, *Phys. Rev.* **112,** 90 (1958).
23. G. V. Lewis and C. R. A. Catlow, *J. Phys. C.* **18,** 1149 (1985).
24. V. Butler, C. R. A. Catlow, B. E. F. Fender, and J. H. Harding, *Solid State Ionics* **8,** 109 (1983).
25. C. R. A. Catlow, *Proc. R. Soc. London, A* **353,** 533 (1977).
26. A. N. Cormack, *Solid State Ionics* **8,** 187 (1983).
27. M. J. Gillan, *Philos. Mag. A* **43,** 301 (1981).
28. C. R. A. Catlow, R. James, W. C. Mackrodt, and R. F. Stewart, *Phys. Rev. B: Condens. Matter* **25,** 1006 (1982).
29. N. F. Mott and M. J. Littleton, *Trans. Faraday Soc.* **34,** 485 (1938).
30. M. J. Norgett, *UKAEA Harwell Report*, AERE-R 7650 (1974).
31. A. J. Lindop, C. Matthews, and D. W. Goodwin, *Acta Crystallogr., Sect. B: Struct. Crystallogr. Cryst. Chem.* **31,** 2940 (1975).
32. P. E. D. Morgan and J. A. Miles, *J. Am. Ceram. Soc.* **69,** C-157 (1986).
33. H. St. C. O'Neil and A. Navrotsky, *Am. Mineral.* **68,** 181 (1983).
34. K. Kato and H. Saalfeld, *Neues Jahrb. Mineral., Abh.* **109,** 192 (1968).
35. A. Utsunomiya, K. Tanaka, H. Morikawa, F. Marumo, and H. Kojima, *J. Solid State Chem.* **75,** 197 (1988).
36. F. Laville, M. Perrin, A. M. Lejus, M. Gasperin, R. Moncorge, and D. Vivien, *J. Solid State Chem.* **65,** 301 (1986).
37. E. Tronc, F. Laville, M. Gasperin, A. M. Lejus, and D. Vivien, *J. Solid State Chem.* **81,** 192 (1989).
38. K. Kimura, M. Ohgaki, K. Tanaka, H. Morikawa, and F. Marumo, *J. Solid State Chem.* **87,** 186 (1990).
39. L. Xie and A. N. Cormack, *J. Solid State Chem.* **83,** 282 (1989).
40. A. N. Cormack, *Adv. Solid-State Chem.* **3,** 63 (1993).
41. D. Gourier, F. Laville, D. Vivien, and C. Valladas, *J. Solid State Chem.* **61,** 67 (1986).
42. D. Gourier, L. Colle, A. M. Lejus, D. Vivien, and R. Moncorge, *J. Appl. Phys.* **63,** 1144 (1988).
43. R. Collongues, D. Gourier, A. Kahn-Harari, A. M. Lejus, J. Thery, and D. Vivien, *Ann. Rev. Mater. Sci.* **20,** 51 (1990).